Mon. Not. R. Astron. Soc. 000, 000–000 (0000) Printed 5 July 1999 (MN LATEX style file v1.4)

The response of a turbulent accretion disc to an imposed epicyclic shearing motion

Ulf Torkelsson[1,2], Gordon I. Ogilvie[1,3,4], Axel Brandenburg[3,5,6], James E. Pringle[1,3], Åke Nordlund[7,8], Robert F. Stein[9]

[1] *Institute of Astronomy, Madingley Road, Cambridge CB3 0HA, United Kingdom*
[2] *Chalmers University of Technology/Göteborg University, Department of Theoretical Physics, Astrophysics Group, S-412 96 Gothenburg, Sweden*
[3] *Isaac Newton Institute for Mathematical Sciences, 20 Clarkson Road, Cambridge CB3 0EH, United Kingdom*
[4] *Max-Planck-Institut für Astrophysik, Karl-Schwarzschild-Straße 1, Postfach 1523, D-85740 Garching bei München, Germany*
[5] *Department of Mathematics, University of Newcastle upon Tyne, NE1 7RU, United Kingdom*
[6] *Nordita, Blegdamsvej 17, DK-2100 Copenhagen Ø, Denmark*
[7] *Theoretical Astrophysics Center, Juliane Maries Vej 30, DK-2100 Copenhagen Ø, Denmark*
[8] *Copenhagen University Observatory, Juliane Maries Vej 30, DK-2100 Copenhagen Ø, Denmark*
[9] *Department of Physics and Astronomy, Michigan State University, East Lansing, MI 48824, USA*

5 July 1999

ABSTRACT

We excite an epicyclic motion, whose amplitude depends on the vertical position, z, in a simulation of a turbulent accretion disc. An epicyclic motion of this kind can be caused by a warping of the disc. By studying how the epicyclic motion freely decays as a result of the turbulence, we estimate the effective viscosity parameter, $\alpha_{\rm v}$, pertaining to such a vertical shear. We also gain new information on the properties of the disc turbulence in general, and measure the usual viscosity parameter, $\alpha_{\rm h}$, pertaining to a horizontal (Keplerian) shear. We find that, as is often assumed in theoretical studies, $\alpha_{\rm v}$ is approximately equal to $\alpha_{\rm h}$ and both are much less than unity. In view of the smallness (~ 0.01) of $\alpha_{\rm v}$ and $\alpha_{\rm h}$ we conclude that the time-scale for diffusion or damping of a warp is much shorter than the usual viscous time-scale, and review the astrophysical implications.

Key words: accretion: accretion discs – MHD – turbulence – instabilities.

1 INTRODUCTION

Warped accretion discs appear in many astrophysical systems. A well known case is the X-ray binary Her X-1, in which a precessing warped disc is understood to be periodically covering our line of sight to the neutron star, resulting in a 35-day periodicity in the X-ray emission (Tananbaum et al. 1972; Katz 1973; Roberts 1974). A similar phenomenon is believed to occur in a number of other X-ray binaries. In recent years the active galaxy NGC 4258 has received much attention as a warp in the accretion disc has been made visible by a maser source (Miyoshi et al. 1995).

A warp may appear in an accretion disc in response to an external perturber such as a binary companion, but it is also possible that the disc can produce a warp on its own. Pringle (1996) showed that the radiation pressure from the central radiation source can produce a warp in the outer disc. In a related mechanism the irradiation can drive an outflow from the disc. The force of the wind can then in a similar way excite a warp in the disc (Schandl & Meyer 1994).

It was shown by Balbus & Hawley (1991) that there is a magnetic shearing instability in Keplerian accretion discs. This instability leads to the appearance of turbulence in the accretion disc. Several numerical simulations (e.g. Hawley, Gammie & Balbus 1995, Matsumoto & Tajima 1995, Brandenburg et al. 1995, Stone et al. 1996) have demonstrated that this turbulence produces Maxwell and Reynolds stresses that transport angular momentum outwards, thus driving the accretion. So far none of the simulations has addressed the question of how the turbulence responds to external perturbations or systematic motions that are more complex than a Keplerian shear flow.

Locally, one of the effects of a warp is to induce an epicyclic motion whose amplitude varies linearly with distance from the midplane of the disc. This motion is driven near resonance in a Keplerian disc, and its amplitude and phase are critical in determining the evolution of the warp (Papaloizou & Pringle 1983; Papaloizou & Lin 1995). The

epicyclic motion is itself a solution of the equations that describe the local hydrodynamics of the accretion disc, and such motions may also be generated spontaneously by turbulence in the accretion disc (e.g. Torkelsson et al. 1997). Just as the turbulence drives accretion by producing a 'viscous' stress in response to the Keplerian shear, the shearing epicyclic motion (and thus the warp) are expected to be damped by the turbulence. However, the details of this process require a numerical investigation.

We start this paper by describing the shearing-box approximation of magnetohydrodynamics and summarizing the properties of the epicyclic motion in a shearing box in Sect. 2. Section 3 is then a description of our simulations of an epicyclic motion. The results of the simulations are then described in Sect. 4 and briefly summarized in Sect. 5.

2 MATHEMATICAL FORMULATION

2.1 The local structure of a steady disc

For the intentions of this paper it is sufficient to use a simple model of the vertical structure of a geometrically thin accretion disc. The disc is initially in hydrostatic equilibrium,

$$\frac{\partial p}{\partial z} = \rho g_z, \tag{1}$$

where p is the pressure, ρ the density, and $g_z = -GMz/R_0^3$ the vertical component of the gravity with G the gravitational constant, M the mass of the accreting star, and R_0 the radial distance from the star. For simplicity we assume that the disc material is initially isothermal, and is a perfect gas, so that $p = c_s^2\rho$, where c_s is the isothermal sound speed, which is initially constant. The density distribution is then

$$\rho = \rho_0 \mathrm{e}^{-z^2/H^2}, \tag{2}$$

where the Gaussian scale height, H, is given by

$$H^2 = \frac{2c_s^2 R_0^3}{GM}. \tag{3}$$

2.2 Epicyclic motion in the shearing box approximation

In the shearing box approximation a small part of the accretion disc is represented by a Cartesian box which is rotating at the Keplerian angular velocity $\Omega_0 = \sqrt{GM/R_0^3}$. The box uses the coordinates (x, y, z) for the radial, azimuthal and vertical directions, respectively. The Keplerian shear flow within the box is $u_y^{(0)} = -\frac{3}{2}\Omega_0 x$, and we solve for the deviations from the shear flow exclusively. The magnetohydrodynamic (MHD) equations can then be written

$$\frac{\mathcal{D}\rho}{\mathcal{D}t} = -\nabla\cdot(\rho\mathbf{u}), \tag{4}$$

$$\frac{\mathcal{D}\mathbf{u}}{\mathcal{D}t} = -(\mathbf{u}\cdot\nabla)\,\mathbf{u} + \mathbf{g} + \mathbf{f}(\mathbf{u}) - \frac{1}{\rho}\nabla p + \frac{1}{\rho}\mathbf{J}\times\mathbf{B} + \frac{1}{\rho}\nabla\cdot(2\nu\rho\mathbf{S}), \tag{5}$$

$$\frac{\mathcal{D}\mathbf{B}}{\mathcal{D}t} = \nabla\times(\mathbf{u}\times\mathbf{B}) - \nabla\times\eta\mu_0\mathbf{J}, \tag{6}$$

$$\frac{\mathcal{D}e}{\mathcal{D}t} = -(\mathbf{u}\cdot\nabla)e - \frac{p}{\rho}\nabla\cdot\mathbf{u} + \frac{1}{\rho}\nabla\cdot(\chi\rho\nabla e) + 2\nu\mathbf{S}^2 + \frac{\eta\mu_0}{\rho}\mathbf{J}^2 + Q, \tag{7}$$

where $\mathcal{D}/\mathcal{D}t = \partial/\partial t + u_y^{(0)}\partial/\partial y$ includes the advection by the shear flow, ρ is the density, $\mathbf{u}$ the deviation from the Keplerian shear flow, p the pressure, $\mathbf{f}(\mathbf{u}) = \Omega_0(2u_y, -\frac{1}{2}u_x, 0)$ the inertial force, $\mathbf{B}$ the magnetic field, $\mathbf{J} = \nabla\times\mathbf{B}/\mu_0$ the current, μ_0 the permeability of free space, ν the viscosity, $S_{ij} = \frac{1}{2}(u_{i,j} + u_{j,i} - \frac{2}{3}\delta_{ij}u_{k,k})$ the rate of strain tensor, η the magnetic diffusivity, e the internal energy, χ the thermal conductivity, and Q is a cooling function. The radial component of the gravity cancels against the centrifugal force, and the remaining vertical component is $\mathbf{g} = -\Omega_0^2 z\hat{\mathbf{z}}$. We adopt the equation of state for an ideal gas, $p = (\gamma - 1)\rho e$.

When the horizontal components of the momentum equation (5) are averaged over horizontal layers (an operation denoted by angle brackets), we obtain

$$\frac{\partial}{\partial t}\langle\rho u_x\rangle = 2\Omega_0\langle\rho u_y\rangle - \frac{\partial}{\partial z}\langle\rho u_x u_z\rangle + \frac{\partial}{\partial z}\left\langle\frac{B_x B_z}{\mu_0}\right\rangle, \tag{8}$$

$$\frac{\partial}{\partial t}\langle\rho u_y\rangle = -\frac{1}{2}\Omega_0\langle\rho u_x\rangle - \frac{\partial}{\partial z}\langle\rho u_y u_z\rangle + \frac{\partial}{\partial z}\left\langle\frac{B_y B_z}{\mu_0}\right\rangle. \tag{9}$$

The explicit viscosity, which is very small, has been neglected here. These equations contain vertical derivatives of components of the turbulent Reynolds and Maxwell stress tensors, distinct from the xy-components that drive the accretion.

We initially neglect the turbulent stresses and obtain the solution

$$\langle\rho u_x\rangle = \rho_0(z)\tilde{u}_0(z)\cos(\Omega_0 t), \tag{10}$$

$$\langle\rho u_y\rangle = -\frac{1}{2}\rho_0(z)\tilde{u}_0(z)\sin(\Omega_0 t), \tag{11}$$

which describes an epicyclic motion. Here $\rho_0(z)$ is the initial density profile. The initial velocity amplitude $\tilde{u}_0$ is an arbitrary function of z. For the simulations in this paper we will take $\tilde{u}_0(z) \propto \sin(kz)$, where $k = \pi/L_z$, and $-\frac{1}{2}L_z \le z \le \frac{1}{2}L_z$ is the vertical extent of our shearing box. This velocity profile is compatible with the stress-free boundary conditions that we employ in our numerical simulations, and gives a fair representation of a linear profile close to the midplane of the disc.

The kinetic energy of the epicyclic motion is not conserved, but the square of the epicyclic momentum

$$E(z,t) = \frac{1}{2}\langle\rho u_x\rangle^2 + 2\langle\rho u_y\rangle^2, \tag{12}$$

is conserved in the absence of turbulent stresses. By multiplying Eq. (8) by $\langle\rho u_x\rangle$, and Eq. (9) by $4\langle\rho u_y\rangle$ we obtain

$$\frac{\partial E}{\partial t} = F_u + F_B, \tag{13}$$

where

$$F_u = -\langle\rho u_x\rangle\frac{\partial}{\partial z}\langle\rho u_x u_z\rangle - 4\langle\rho u_y\rangle\frac{\partial}{\partial z}\langle\rho u_y u_z\rangle \tag{14}$$

and

$$F_B = \langle\rho u_x\rangle\frac{\partial}{\partial z}\left\langle\frac{B_x B_z}{\mu_0}\right\rangle + 4\langle\rho u_y\rangle\frac{\partial}{\partial z}\left\langle\frac{B_y B_z}{\mu_0}\right\rangle \tag{15}$$

represent the 'rates of working' of the Reynolds and Maxwell stresses, respectively, on the epicyclic oscillator. We may expect that both F_u and F_B are negative, but by measuring them in the simulation we can determine the relative importance of the Reynolds and Maxwell stresses in damping the

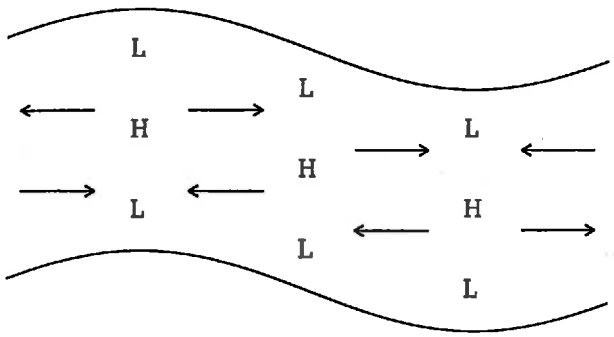

Figure 1. Owing to the stratification there appear horizontal pressure gradients in the warped disc. These gradients excite the epicyclic motion (arrows indicate forces, not velocities)

epicyclic motion. We will also refer to an epicyclic velocity amplitude

$$\tilde{u} = \sqrt{\langle u_x\rangle^2 + 4\langle u_y\rangle^2}. \tag{16}$$

2.3 Theoretical expectations

The detailed fluid dynamics of a warped accretion disc has been discussed by, e.g., Papaloizou & Pringle (1983), Papaloizou & Lin (1995) and Ogilvie (1999). The dominant motion is circular Keplerian motion, but the orbital plane varies continuously with radius r and time t. This may conveniently be described by the tilt vector $\boldsymbol{\ell}(r,t)$, which is a unit vector parallel to the local angular momentum of the disc annulus at radius r. A dimensionless measure of the amplitude of the warp is then $A = |\partial\boldsymbol{\ell}/\partial\ln r|$.

In the absence of a detailed understanding of the turbulent stresses in an accretion disc, it is often assumed that the turbulence acts as an isotropic effective viscosity in the sense of the Navier-Stokes equation. The dynamic viscosity may be parametrized as

$$\mu = \alpha p/\Omega_0, \tag{17}$$

where α is a dimensionless parameter (Shakura & Sunyaev 1973). In this paper we will allow, in a simple way, for the possibility that the effective viscosity is anisotropic (cf. Terquem 1998). The parameter α_h pertaining to 'horizontal' shear (i.e. horizontal-horizontal components of the rate-of-strain tensor, such as the Keplerian shear) may be different from the parameter α_v pertaining to 'vertical' shear (i.e. horizontal-vertical components of the rate-of-strain tensor, such as the shearing epicyclic motion).

Owing to the stratification of pressure resulting from vertical hydrostatic equilibrium, in a warped disc there are also *horizontal* pressure gradients (Fig. 1). The horizontal accelerations are of order $A\Omega_0^2 z$ and oscillate at the local orbital frequency, as viewed in a frame co-rotating with the fluid. They drive epicyclic motions of the type studied in this paper, which are shearing in the vertical direction and are therefore acted on by the effective turbulent viscosity. In a Keplerian disc the driving frequency coincides with the natural frequency of the epicyclic motion, and a resonance occurs. In the case $H/r \lesssim \alpha_\mathrm{v} \ll 1$ (Papaloizou & Pringle 1983) the resulting amplitude of the epicyclic motions is determined by a simple balance between forcing and viscous damping, and is given by

$$u_x \propto u_y \propto \frac{A\Omega_0 z}{\alpha_\mathrm{v}}. \tag{18}$$

The resulting hydrodynamic stresses $\overline{\rho u_x u_z}$ and $\overline{\rho u_y u_z}$ (overbars denote averages over the orbital time-scale), which tend to flatten out the disc, are also proportional to $\alpha_\mathrm{v}^{-1}A$ and therefore dominate over the direct viscous stresses $\propto \alpha_\mathrm{v} A$ which would have the same effect. It is for this reason that the time-scale for flattening a warped disc is anomalously short compared to the usual viscous time-scale, by a factor of approximately $2\alpha_\mathrm{h}\alpha_\mathrm{v}$. (For more details, see Papaloizou & Pringle 1983 and Ogilvie 1999. In these papers it was assumed that $\alpha_\mathrm{h} = \alpha_\mathrm{v}$.)

In the formulation of Pringle (1992) there are two different effective kinematic viscosity coefficients: ν_1 describes the radial transport of the aligned component of the angular momentum vector, while ν_2 describes the transport of the misaligned components. In this notation we should have $\nu_2/\nu_1 \approx 1/(2\alpha_\mathrm{h}\alpha_\mathrm{v})$. It is important to realize that, even in the case of an isotropic underlying viscous process ($\alpha_\mathrm{h} = \alpha_\mathrm{v}$), $\nu_2 \neq \nu_1$, in particular ν_2 is greatly enhanced by the resonant effects described above if $\alpha_\mathrm{v} \ll 1$.

We aim to measure both α_h and α_v in the simulations. The first may be obtained through the relation

$$\left\langle \rho u_x u_y - \frac{B_x B_y}{\mu_0} \right\rangle_\mathrm{V} = \frac{3}{2}\alpha_\mathrm{h}\langle p\rangle_\mathrm{V}, \tag{19}$$

which follows by identifying the total turbulent xy-stress with the effective viscous xy-stress resulting from the viscosity (17) acting on the Keplerian shear (note that the definition of α_h differs from that of α_SS in Brandenburg et al. 1995 by a factor $\sqrt{2}$). Here the average is over the entire computational volume.

The coefficient α_v may be obtained by measuring the damping time of the epicyclic motion. In the shearing-box approximation the horizontal components of the Navier-Stokes equation for a free epicyclic motion decaying under the action of viscosity are

$$\frac{\partial u_x}{\partial t} = 2\Omega_0 u_y + \frac{1}{\rho}\frac{\partial}{\partial z}\left(\frac{\alpha_\mathrm{v} p}{\Omega_0}\frac{\partial u_x}{\partial z}\right), \tag{20}$$

$$\frac{\partial u_y}{\partial t} = -\frac{1}{2}\Omega_0 u_x + \frac{1}{\rho}\frac{\partial}{\partial z}\left(\frac{\alpha_\mathrm{v} p}{\Omega_0}\frac{\partial u_y}{\partial z}\right). \tag{21}$$

Under the assumptions that α_v and $\partial_z \mathrm{u}$ are independent of z and that the disc is vertically in hydrostatic equilibrium, these equations have the exact solution

$$u_x = C\Omega_0 z\,\mathrm{e}^{-t/\tau}\cos(\Omega_0 t), \tag{22}$$

$$u_y = -\frac{1}{2}C\Omega_0 z\,\mathrm{e}^{-t/\tau}\sin(\Omega_0 t), \tag{23}$$

where C is a dimensionless constant and

$$\tau = \frac{1}{\alpha_\mathrm{v}\Omega_0} \tag{24}$$

is the damping time. Admittedly it is already believed that α_h is not independent of z (Brandenburg et al. 1996) and therefore α_v may not be either. Also our velocity profile is not exactly proportional to z. However, it is in fact the damping time that matters for the application to warped

Table 1. Specification of numerical simulations: the number of grid points are given by $N_x \times N_y \times N_z$, and the amplitude of the initial velocity perturbation is u_0

Run	$N_x \times N_y \times N_z$	u_0
0	31 × 63 × 63	0.0
1	31 × 63 × 63	0.011
1b	63 × 127 × 127	0.011
2	31 × 63 × 63	0.095
3	63 × 127 × 127	0.095

discs, and the solution that we describe above is in a sense the fundamental mode of the epicyclic shear flow in a warped disc.

A further theoretical expectation is as follows. In an inviscid disc, the epicyclic motion can decay by exciting inertial waves through a parametric instability (Gammie, Goodman & Ogilvie 1999, in preparation). In the optimal case, the signature of these waves is motion at 30° to the vertical, while the wave vector is inclined at 60° to the vertical. The characteristic local growth rate of the instability is

$$\gamma = \frac{3\sqrt{3}}{16}\left|\frac{\partial \tilde{u}}{\partial z}\right|. \tag{25}$$

This instability can lead to a rapid damping of a warp, but may be somewhat delicate as it relies on properties of the inertial-wave spectrum. It is important to determine whether it occurs in the presence of MHD turbulence.

3 NUMERICAL SIMULATIONS

3.1 Computational method

We use the code by Nordlund & Stein (1990) with the modifications that were described by Brandenburg et al. (1995). The code solves the MHD equations for $\ln \rho$, $\mathbf{u}$, e and the vector potential $\mathbf{A}$, which gives the magnetic field via $\mathbf{B} = \nabla \times \mathbf{A}$. For the (radial) azimuthal boundaries we use (sliding-) periodic boundary conditions. The vertical boundaries are assumed to be impenetrable and stress-free. Unlike our earlier studies, we now adopt perfectly conducting vertical boundary conditions for the magnetic field. Thus we have

$$\frac{\partial u_x}{\partial z} = \frac{\partial u_y}{\partial z} = u_z = 0, \tag{26}$$

and

$$\frac{\partial B_x}{\partial z} = \frac{\partial B_y}{\partial z} = B_z = 0. \tag{27}$$

We choose units such that $H = GM = 1$. Density is normalized so that initially $\rho = 1$ at the midplane, and we measure the magnetic field strength in velocity units, which allows us to set $\mu_0 = 1$. The disc can be considered to be thin by the assumptions of our model, and the results will thus not depend on the value of R_0. We choose to set $R_0 = 10$ in our units, which gives the orbital period $T_0 = 2\pi/\Omega_0 = 199$, and the mean internal energy $7.4\,10^{-4}$. The size of the box is $L_x : L_y : L_z = 1 : 2\pi : 4$, where x and z vary between $\pm\frac{1}{2}L_x$ and $\pm\frac{1}{2}L_z$, respectively, and y goes from 0 to L_y. The number of grid points is $N_x \times N_y \times N_z$. To stop the box from heating up during the simulation we introduce the cooling function

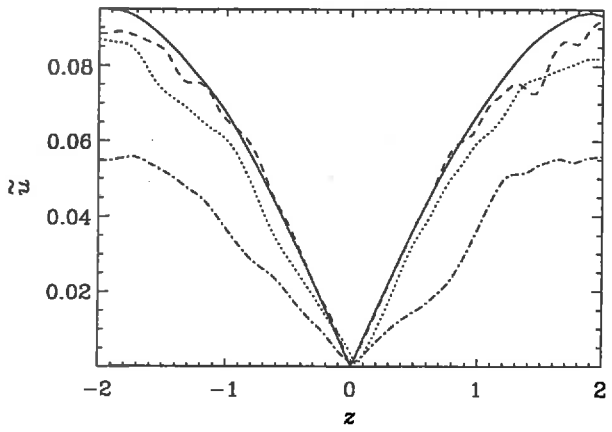

Figure 2. $\tilde{u}$ as a function of z at $t = 55.8\,T_0$ (solid line), $57.1\,T_0$ (dashed line), $58.4\,T_0$ (dotted line), and $60.9\,T_0$ (dot-dashed line) for Run 3

$$Q = -\sigma_{\rm cool}\,(e - e_0)\,, \tag{28}$$

where $\sigma_{\rm cool}$ is the cooling rate, which typically corresponds to a time-scale of 1.5 orbital periods, and e_0 is the internal energy of an isothermal disc.

We start the simulations from a snapshot of a previous simulation in which turbulence has already developed. For every horizontal layer in the snapshot we subtract the mean horizontal velocity and then add a net radial flow of the form

$$u_r = u_0 \sin\left(\frac{\pi z}{L_z}\right). \tag{29}$$

The number of grid points and u_0 for the different runs are given in Table 1. u_0 should be compared to the adiabatic sound speed which is 0.029. We include one run, Run 0, in which we do not excite an epicyclic motion, as a reference.

3.2 Results

We concentrate on Run 3, which has the highest resolution and an epicyclic motion of large amplitude. We show the vertical variation of $\tilde{u}$ at four different times in Fig. 2, and plot it as a function of time on three planes, $z = 1.52$, $z = 0.89$ and $z = 0.44$, in Fig. 3. Figure 2 shows that the damping sets in first at the surfaces, while for $|z| < 1$ there is essentially no damping during the first two orbital periods (Fig. 3). There is then a brief period of rapid damping between $t = 58\,T_0$ and $t = 60\,T_0$ throughout the box, especially for small $|z|$ where $\tilde{u}$ may drop by a factor 2. This is followed by a period of exponential decay, but after $t = 75\,T_0$ it becomes difficult to follow the epicyclic motion, as the influence of the random turbulence on $\tilde{u}$ becomes significant, in particular close to the midplane, where $\tilde{u}$ is anyway small. We estimate the damping time, $\tau = (\mathrm{d}\ln\tilde{u}/\mathrm{d}t)^{-1}$ by fitting exponentials to $\tilde{u}$ in the interval $60T_0 < t < 75T_0$. Averaged over the box we get $\tau = 25 \pm 8T_0$, which corresponds to $\alpha_{\rm v} = 0.006$ according to Eq. (24).

We can determine the influence of the Maxwell and Reynolds stresses on the shear flow, by plotting F_u and F_B as functions of time (Fig. 4). The surprising result is that the epicyclic motion is damped by the Reynolds stress, while,

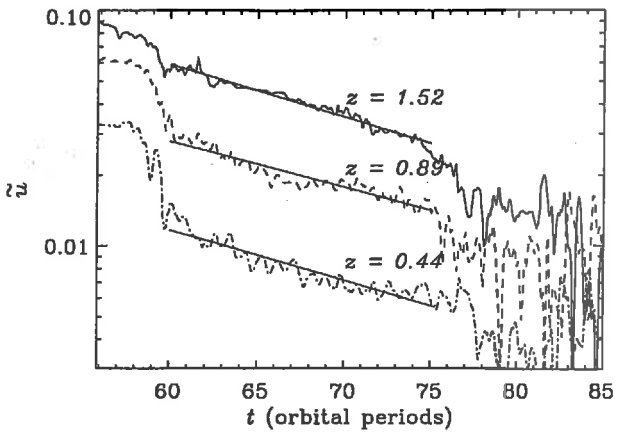

Figure 3. The amplitude of the epicyclic motion in Run 3, $\tilde{u}$, as a function of t on three horizontal planes: $z = 1.52$ (solid line), $z = 0.89$ (dashed line) and $z = 0.44$ (dot-dashed line). The straight lines are exponential functions that have been fitted for the interval $60T_0 < t < 75T_0$. The e-folding time scales of the exponentials starting from the top are $19.4T_0$, $22.1T_0$ and $20.2T_0$, respectively. The epicyclic motion was added to the box at $t = 55.7\,T_0$

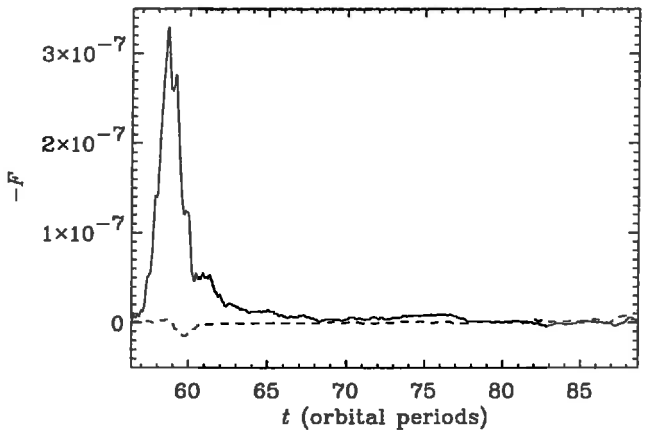

Figure 4. The moving averages (over one orbital period)of the vertical averages of $-F_u$ (solid line) and $-F_B$ (dashed line)

as we will see below, the accretion is driven largely by the Maxwell stress.

The accretion itself is driven by the $\langle \rho u_x u_y - B_x B_y \rangle$-stresses. We plot the moving time-averages of the vertical average of the accretion-driving stress of Run 3 in Fig. 5, and as a comparison that of Run 0 in Fig. 6. In the beginning of Run 3 the Reynolds stress is modulated on half of the orbital period. This modulation is an artefact of the damping of the epicyclic motion and dies out with time. The Maxwell stress becomes significantly stronger than the Reynolds stress once the epicyclic motion has vanished. Later the stresses vary in phase which each other, like they do all the time in Run 0. The main difference between Run 0 and the end of Run 3 is that the stresses are 2-3 times larger in Run 3. We calculate $\alpha_{\rm h}$ for Run 3 by dividing the stresses by $\frac{3}{2}\overline{\langle p \rangle}_{\rm V}$ (Fig. 7).

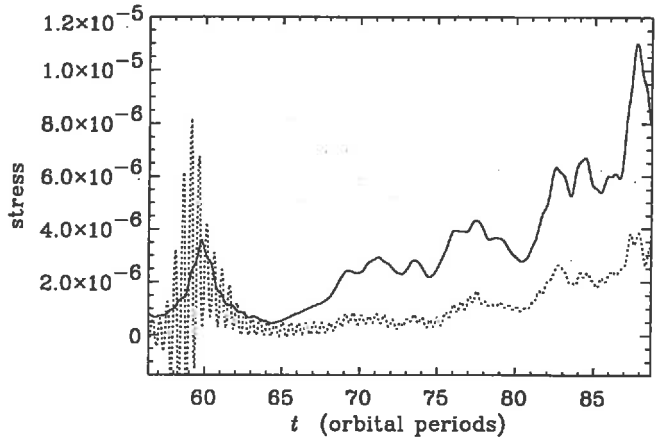

Figure 5. The moving averages (over one orbital period) of the vertical averages of $-\langle B_x B_y \rangle$ (solid line) and $\langle \rho u_x u_y \rangle$ of Run 3

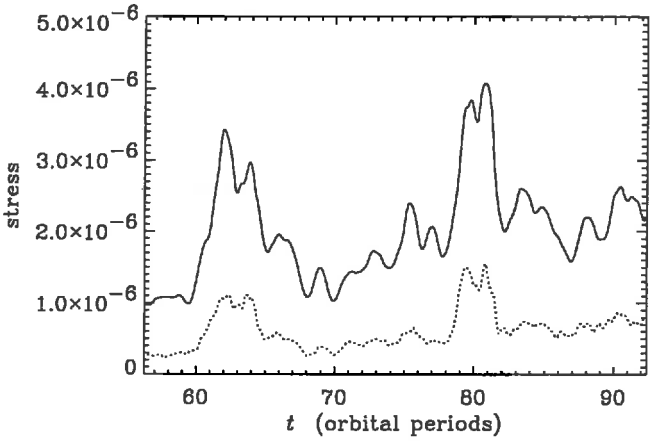

Figure 6. The moving averages (over one orbital period) of the vertical averages of $-\langle B_x B_y \rangle$ (solid line) and $\langle \rho u_x u_y \rangle$ of Run 0

One should take note that the simulations in this paper are too short to derive $\alpha_{\rm h}$ with high statistical significance (cf. Brandenburg et al. 1995), but our results do show that $\alpha_{\rm h}$ varies in phase with the stress. In other words the pressure variations are smaller (the pressure increases with 50% during the course of the simulation) than the stress variations, which is not what we expect from Eq. (19). The lack of a correlation between the stress and the pressure is even more evident in Run 0, in which the pressure never varies with more than 5%.

In our previous work (Brandenburg et al. 1995) we found that the toroidal magnetic flux reversed its direction about every 30 orbital periods. With the perfect conductor boundary conditions that we have assumed in this paper such field reversals are not allowed, since the boundary conditions conserve the magnetic flux (e.g. Brandenburg 1999). However the azimuthal magnetic field is organised in such a way that it is antisymmetric with respect to the midplane. We find one example of a reversal of the azimuthal magnetic field in Run 3 (Fig. 8).

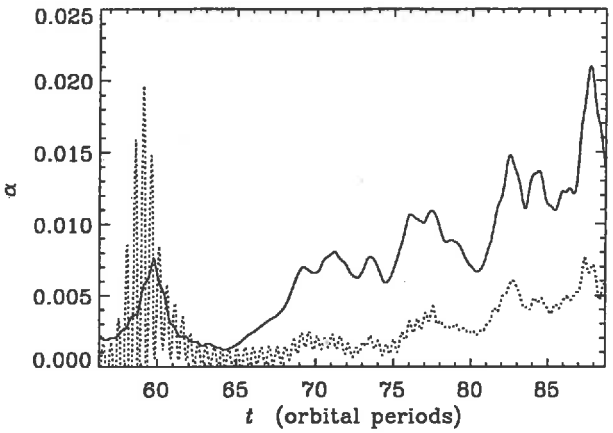

Figure 7. $\alpha_{\rm h}$ is calculated by dividing the moving averages (over one orbital period) of the vertical averages of $-\langle B_x B_y \rangle$ (solid line) and $\langle \rho u_x u_y \rangle$ (dashed line) of Run 3 with the moving average of $\langle p \rangle_{\rm V}$

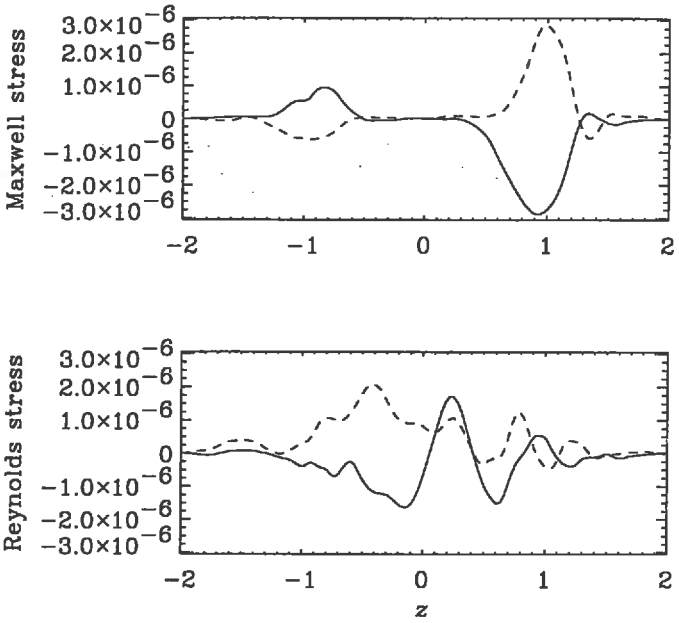

Figure 9. The Maxwell (top) and Reynolds (bottom) stresses averaged over one orbital period at 76.3 T_0 of Run 3. The yz-stresses are plotted with solid lines and the zx-stresses with dashed lines

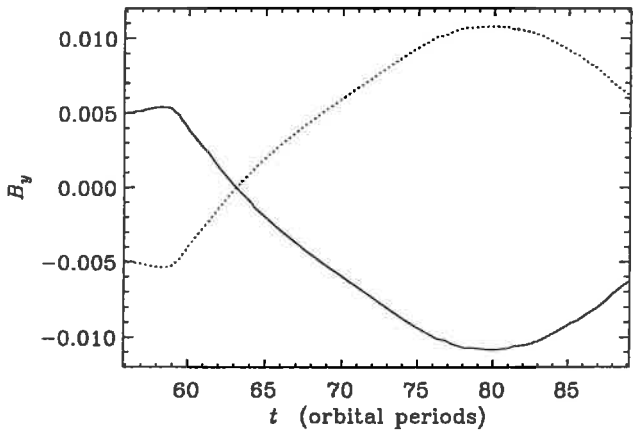

Figure 8. B_y averaged over the upper half (solid line) and lower half (dotted line) of the box of Run 3

3.3 Dependence on u_0 and on the resolution

There is no clear dependence of the damping time-scale on u_0, but it is more difficult to study the damping of the epicyclic motion for a smaller u_0, as the turbulence can excite epicyclic motions on its own. These randomly excited motions swamp the epicyclic motion that we are studying. The quantitative results from Runs 1 and 1b are therefore more uncertain, but qualitatively the damping behaves in the same way as in Run 3, and within the uncertainties the damping time-scale is the same. In other respects the turbulent stresses of Runs 1 and 1b are more similar to those of Run 0 than to those of Run 3.

On the other hand there are significant differences between Runs 2 and 3, which differ only in terms of the grid resolution. The magnetic field decays rapidly in Run 2, and only the toroidal field recovers towards the end of the simulation. In the absence of a poloidal magnetic field there is no magnetic stress, and therefore the disc cannot derive energy from the shear flow. Consequently there is no turbulent heating in Run 2, and the disc settles down to an isothermal state. Apparently the turbulence is killed by the numerical diffusion in Run 2. This demonstrates that the minimal resolution, which is required in the simulation, depends on the amplitude of $\tilde{u}_0$. A simulation with an imposed velocity $\tilde{u}_0$ with an amplitude significantly larger than that of the turbulence requires a finer resolution than a simulation of undisturbed turbulence. Run 2 failed because it did not have sufficient resolution to resolve the imposed velocity field. This was not a problem in Run 1, where the amplitude of $\tilde{u}_0$ is much smaller.

4 DISCUSSION

4.1 Statistical properties of the turbulent stress

Figure 9 shows the Maxwell and Reynolds stresses at 76.3 T_0, that is after that the epicyclic motion has been damped out. The $\overline{\langle B_y B_z \rangle}$- and $\overline{\langle B_z B_x \rangle}$-stresses are clearly anti-correlated at this moment. We define the correlations

$$\chi_u = \frac{\int \overline{\langle \rho u_x u_z \rangle \langle \rho u_y u_z \rangle} \mathrm{d}z}{\int \left(\overline{\langle \rho u_x u_z \rangle}^2 + \overline{\langle \rho u_y u_z \rangle}^2 \right) \mathrm{d}z}, \tag{30}$$

and

$$\chi_B = \frac{\int \overline{\langle B_x B_z \rangle \langle B_y B_z \rangle} \mathrm{d}z}{\int \left(\overline{\langle B_x B_z \rangle}^2 + \overline{\langle B_y B_z \rangle}^2 \right) \mathrm{d}z}, \tag{31}$$

which are -0.5 if the stresses are completely anti-correlated, and 0.5 if they are completely correlated, and plot them together with the stresses in Fig. 10. The Reynolds stresses

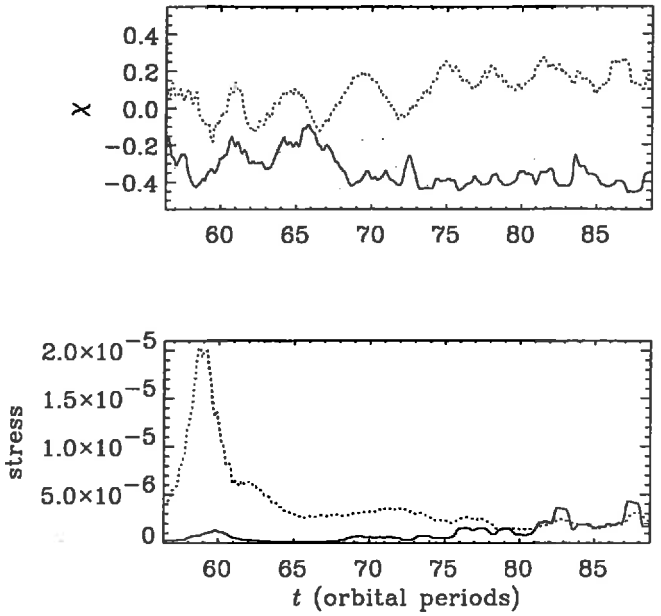

Figure 10. The upper plot shows χ_B (solid line) and χ_u (dashed line) as functions of time for Run 3. The lower plot shows the vertical averages of $\overline{\langle B_y B_z\rangle^2 + \langle B_z B_x\rangle^2}^{1/2}$ (solid line) and $\overline{\langle \rho u_y u_z\rangle^2 + \langle \rho u_z u_x\rangle^2}^{1/2}$ (dashed line)

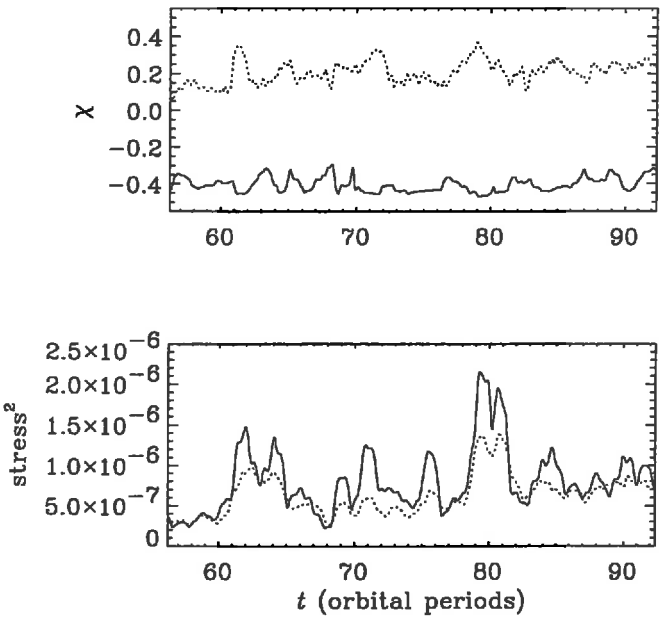

Figure 11. Same as Fig. 10, but for Run 0. The upper plot shows χ_B (solid line) and χ_u (dashed line) and the lower plot the vertical averages of $\overline{\langle B_y B_z\rangle^2 + \langle B_z B_x\rangle^2}^{1/2}$ (solid line) and $\overline{\langle \rho u_y u_z\rangle^2 + \langle \rho u_z u_x\rangle^2}^{1/2}$ (dashed line)

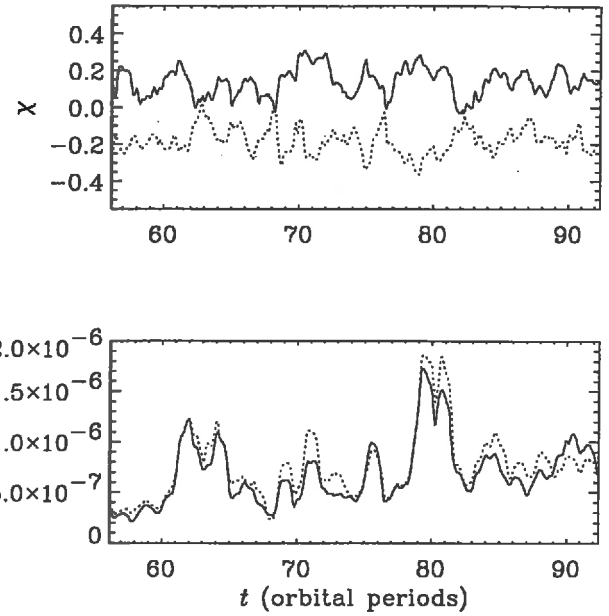

Figure 12. The upper plot shows the vertically averaged cross correlations between the Maxwell and Reynolds stresses, $\overline{\langle \rho u_x u_z\rangle\langle B_y B_z\rangle}$ (solid line) and $\overline{\langle \rho u_y u_z\rangle\langle B_x B_z\rangle}$ (dashed line) for Run 0. The lower plot shows the vertical averages of $\overline{\langle B_y B_z\rangle^2 + \langle \rho u_x u_z\rangle^2}^{1/2}$ (solid line) and $\overline{\langle B_x B_z\rangle^2 + \langle \rho u_y u_z\rangle^2}^{1/2}$ (dashed line)

are much larger than the Maxwell stresses, and χ_u is fluctuating around 0 while the epicyclic motion is damped. Late in the simulation the Maxwell and Reynolds stresses are of comparable magnitude, but the Maxwell stresses are anti-correlated while the Reynolds stresses are weakly correlated. The cross-correlation terms $\overline{\langle \rho u_x u_z\rangle\langle B_y B_z\rangle}$ and $\overline{\langle \rho u_y u_z\rangle\langle B_x B_z\rangle}$ are essentially 0. It is a characteristic property of the turbulence even in the absence of an epicyclic motion that the $\langle B_y B_z\rangle$- and $\langle B_z B_x\rangle$-stresses are strongly anti-correlated, while the $\langle \rho u_y u_z\rangle$- and $\langle \rho u_z u_x\rangle$-stresses show a weak correlation (Fig. 11). We note though that the cross-correlations $\overline{\langle \rho u_x u_z\rangle\langle B_x B_z\rangle}$ and $\overline{\langle \rho u_y u_z\rangle\langle B_y B_z\rangle}$ are not 0 in Run 0, rather their correlation coefficients differ by a sign (Fig. 12).

The anti-correlation of the stresses is compatible with an exponential damping of the epicyclic motion as we will now show. Based on Eqs. (10) and (11) we can write $\langle \rho u_x\rangle = \tilde{u}_0 \rho \cos(\Omega_0 t) \mathrm{e}^{-t/\tau}$ and $\langle \rho u_y\rangle = -\frac{1}{2}\tilde{u}_0 \rho \sin(\Omega_0 t) \mathrm{e}^{-t/\tau}$, where ρ has been assumed to be constant over horizontal layers. These expressions can be substituted into Eqs. (8) and (9), which are then multiplied together and averaged over an orbital period

$$\overline{\frac{\partial}{\partial z}\langle \rho u_x u_z - B_x B_z\rangle \frac{\partial}{\partial z}\langle \rho u_y u_z - B_y B_z\rangle} = -\frac{1}{8}\frac{\tilde{u}_0^2 \rho^2 \Omega_0}{\tau^2}\frac{1-\mathrm{e}^{-4\pi/(\tau\Omega_0)}}{\Omega_0^2 + 1/\tau^2}. \quad (32)$$

This equation shows that an anti-correlation of the zx- and yz-stresses will lead to an exponential damping of the epicyclic motion, while a correlation of the stresses will result in an exponential growth. We emphasize though that it

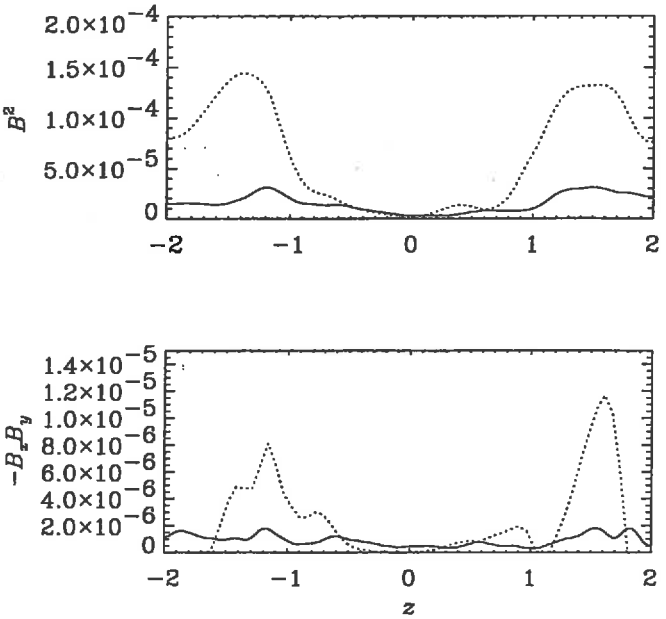

Figure 13. The upper plot shows $\overline{\langle B^2 \rangle}$ the average of the magnetic energy as a function of z for Runs 3 at $66.3T_0$ (solid line) and 0 at $66.1T_0$ (dashed line). The lower plot shows $-\overline{\langle B_x B_y \rangle}$ plotted the same way

is not the Maxwell stress that is damping the epicyclic motion, but rather the Reynolds stress. The anti-correlation of the Maxwell stresses rather explains why the turbulence on its own does not excite a strong, long-lived epicyclic motion, although such a motion is a solution of the MHD-equations for the shearing box.

4.2 The vertical structure of the accretion disc

Our previous simulations of turbulence in a Keplerian shearing box have shown that the turbulent xy-stresses are approximately constant with height (Brandenburg et al. 1996) rather than proportional to the pressure as was predicted by the α-prescription (Shakura & Sunyaev 1973). We modified the vertical boundary conditions for this paper and have added an epicyclic motion. The $\langle B_x B_y \rangle$-stress is still approximately independent of z or even increasing with $|z|$ for $|z| < H$ though, while at larger $|z|$ we may see the effects of the boundary conditions (Fig. 13). The effect of the epicyclic motion is seemingly to limit the $\langle B_x B_y \rangle$-stress in the surface layers to its value in the interior of the disc. The fact that the stresses decrease with z more slowly than the density results in a strong heating of the surface layers, which are the hottest parts of the accretion disc in our simulations.

4.3 Application to warped accretion discs

In linear theory we can estimate the amplitude of the epicyclic motion in a warped accretion disc as (cf. Eq. 18)

$$\frac{u_0}{c_s} \sim \frac{A}{\alpha_{\rm v}}. \tag{33}$$

This estimate is valid for a thin and sufficiently viscous disc, that is for $H/r \lesssim \alpha_{\rm v} \ll 1$ (Papaloizou & Pringle 1983). For observable warps in which the amplitude A exceeds the aspect ratio of the disc, the epicyclic flow can become transonic. One might then expect that shocks would appear, which would enhance the dissipation rate. The analyses by Papaloizou & Pringle (1983) and Ogilvie (1999) would then not be applicable. However, we have found that even a transonic epicyclic motion, as in Run 3, is subject to a smooth 'viscous' damping without shocks.

The condition for a warp to appear in the accretion disc is set by the balance between the torque that is exciting the warp and the viscous torque, described by ν_2, that is flattening the disc. The warp-exciting torque may for instance be a radiation torque from the central radiation source. Assuming that accretion is responsible for all the radiation, the radiation torque will depend on the viscosity ν_1. The criterion for the warp to appear will then depend on the ratio of viscosities $\eta = \nu_2/\nu_1$. Pringle (1996) showed that an irradiation-driven warp will appear at radii

$$r \gtrsim \left(\frac{2\sqrt{2}\pi\eta}{\epsilon} \right)^2 R_{\rm Sch}, \tag{34}$$

where $R_{\rm Sch}$ is the Schwarzschild radius, and $\epsilon = L/\dot{M}c^2$ is the efficiency of the accretion process. We have shown that $\alpha_{\rm h} \approx \alpha_{\rm v} \ll 1$. However, we emphasize again that this does *not* imply that $\eta \approx 1$; on the contrary, we estimate that $\eta \approx 1/(2\alpha_{\rm h}\alpha_{\rm v}) \gg 1$. The reason is that the effective kinematic viscosity ν_2, which parametrizes the stress that acts to flatten out the disc, is in reality not a direct 'viscous' stress (which would be proportional to $\alpha_{\rm v}$) but a hydrodynamic stress mediated by horizontal motions that are *inversely* proportional to $\alpha_{\rm v}$. The high value for η will make it difficult for a warp to appear unless the radiation torque can be amplified by an additional physical mechanism. One way to produce a stronger torque is if the irradiation is driving an outflow from the disc (cf. Schandl & Meyer 1994).

A similar damping mechanism will work on the waves that can be excited by Lense-Thirring precession in the inner part of the accretion disc around a spinning black hole. Numerical calculations by Markovic & Lamb (1998) and Armitage & Natarajan (1999) show that these waves are damped rapidly unless $\nu_2 \ll \nu_1$, which we find is not the case (however, we note that the resonant enhancement of ν_2 will be reduced near the innermost stable circular orbit, because the epicyclic frequency deviates substantially from the orbital frequency). Likewise a high value of ν_2 will lead to a rapid alignment of the angular momentum vectors of a black hole and its surrounding accretion disc (cf. Natarajan & Pringle 1998).

We suggest some caution in interpreting the results of this paper. Although the shearing box simulations in general have been successful in demonstrating the appearance of turbulence with the right properties for driving accretion, they are in general producing uncomfortably low values of $\alpha_{\rm h}$ to describe for instance outbursting dwarf nova discs (e.g. Cannizzo, Wheeler & Polidan 1986). An underestimate of $\alpha_{\rm h}$ and $\alpha_{\rm v}$ would lead to an overestimate of η. In addition we have studied a free-decay problem which differs somewhat from the forced oscillations that occur in warped discs. We postpone the study of forced oscillations to future work.

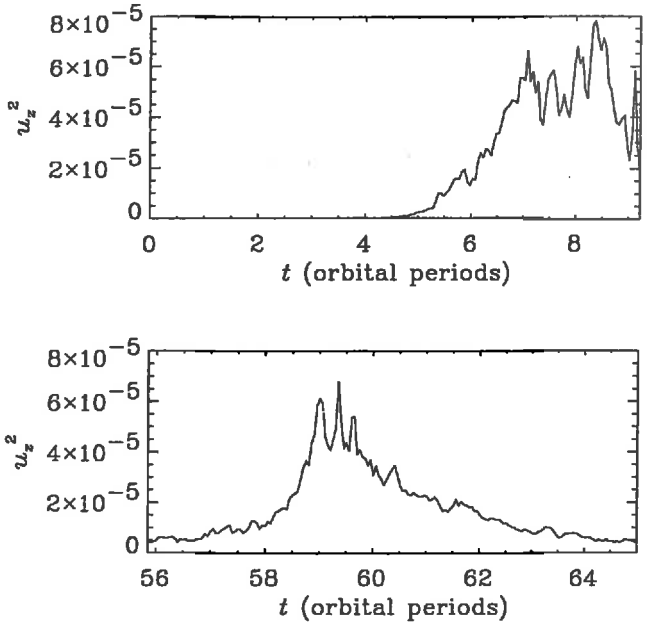

Figure 14. The volume average of u_z^2 for a two-dimensional hydrodynamic simulation (top) and for our three-dimensional magnetohydrodynamic simulation Run 3 (bottom)

4.4 Parametric decay to inertial waves

Gammie et al. (1999) have predicted the occurrence of a parametric instability in the epicyclic shear flow. The shear flow should excite inertial waves that are propagating at a 30° angle to the vertical. Individual inertial waves can be identified by the pattern they form in the helicity, but the parametric instability forms pairs of waves with opposite helicities, which makes them difficult to identify.

To understand the dynamics of the parametric instability we have run a two-dimensional hydrodynamic simulation of the epicyclic shear flow. Our two-dimensional xz-plane has the same extension as in the previous three-dimensional simulations, but we are now using 128×255 grid points. The initial state is a stratified Keplerian accretion disc to which we have added a radial motion with an amplitude of 0.095, and a small random perturbation of the pressure. The most characteristic property of the instability is that a vertical velocity is generated (Fig. 14 top). A similar increase of the vertical velocity appears in Run 3 during the damping of the epicyclic motion (Fig. 14 bottom). The main difference is that the vertical velocities appear faster in Run 3, which can be explained by that the turbulence provides large initial perturbations from which the instability can grow.

5 CONCLUSIONS

In this paper we have studied how the turbulence in an accretion disc will damp an epicyclic motion, whose amplitude depends on the vertical coordinate z in the accretion disc. Such a motion could be set up by a warp in the accretion disc (Papaloizou & Pringle 1983). We find that the typical damping time-scale of the epicyclic motion is about 25 orbital periods, which corresponds to $\alpha_{\rm v} = 0.006$. This value is comparable to the traditional estimate of $\alpha_{\rm h}$ that one gets from comparing the $\langle \rho u_x u_y - B_x B_y \rangle$-stress with the pressure. Both alphas are of the order of 0.01, which implies that the time-scale for damping a warp in the accretion disc is much shorter than the usual viscous time-scale. That the two alphas are within a factor of a few of each other is surprising as the damping of the epicyclic motion can be attributed to the Reynolds stresses, while the accretion is mostly driven by the Maxwell stress.

ACKNOWLEDGMENTS

UT was supported by an EU post-doctoral fellowship in Cambridge and is supported by the Natural Sciences Research Council (NFR) in Gothenburg. Computer resources from the National Supercomputer Centre at Linköping University are gratefully acknowledged. GIO is supported by the European Commision through the TMR network 'Accretion on to Black Holes, Compact Stars and Protostars' (contract number ERBFMRX-CT98-0195). This work was supported in part by the Danish National Research Foundation through its establishment of the Theoretical Astrophysics Center (ÅN). RFS is supported by NASA grant NAG5-4031.

REFERENCES

Armitage, P. J., Natarajan, P., 1999, ApJ, submitted
Balbus S. A., Hawley J. F., 1991, ApJ, 376, 214
Balbus, S. A., Hawley, J. F., 1998, Rev. Mod. Phys., 70, 1
Brandenburg, A., 1999, in M. A. Abramowicz, G. Björnsson & J. E. Pringle (eds.) *Theory of black hole accretion discs*, Cambridge University Press, 61
Brandenburg A., Nordlund Å., Stein R. F., Torkelsson U., 1995, ApJ, 446, 741
Brandenburg A., Nordlund Å., Stein R. F., Torkelsson U., 1996, in S. Kato et al. (eds.), *Basic physics of accretion disks*, Gordon & Breach Sci. Publ., 285
Cannizzo, J. K., Wheeler, J. C., Polidan, R. S., 1986, ApJ, 301, 634
Gammie C. F., Goodman J., Ogilvie G. I., 1999, in preparation
Hawley J. F., Gammie C. F., Balbus S. A., 1995, ApJ, 440, 742
Katz, J. I., 1973, Sci., 246, 87
Markovic, D., Lamb, F. K., 1998, ApJ, 507, 316
Matsumoto R., Tajima T., 1995, ApJ, 445, 767
Miyoshi, M., Moran, J., Herrnstein, J., Greenhill, L., Nakai, N., Diamond, P., Inoue, M., 1995, Nat, 373, 127
Natarajan, P., Pringle, J. E., 1998, ApJ, 506, L97
Nordlund Å., Stein R. F., 1990, Comput. Phys. Commun., 59, 119
Ogilvie, G. I., 1999, MNRAS, 304, 557
Papaloizou J. C. B., Lin D. N. C., 1995, ApJ, 438, 841
Papaloizou J. C. B., Pringle J. E., 1983, MNRAS, 202, 1181
Pringle, J. E., 1992, MNRAS, 258, 811
Pringle J. E., 1996, MNRAS, 281, 357
Roberts, W. J., 1974, ApJ, 187, 575
Schandl, S., Meyer, F., 1994, A&A, 289, 149
Shakura, N. I., Sunyaev, R. A., 1973, A&A, 24, 337
Stone J. M., Hawley J. H., Gammie C. F., Balbus S. A., 1996, ApJ, 463, 656
Tananbaum H., Gursky H., Kellogg E. M., Levinson R., Schreier E., Giacconi R., 1972, ApJ, 174, L143
Terquem, C. E. J. M. L. J., 1998, ApJ, 509, 819
Torkelsson U., Brandenburg A., Nordlund Å., Stein R. F., 1997, in D. T. Wickramasinghe, L. Ferrario & G. V Bicknell (eds.)

Accretion phenomena and related outflows. IAU Coll. 163,
ASP Conf. Ser., Vol 121, 210